Photofragment imaging of methane

Albert J. R. Heck
Combustion Research Facility, Sandia National Laboratories, Livermore, California 94551 and Department of Chemistry, Stanford University, Stanford, California 94305

Richard N. Zare
Department of Chemistry, Stanford University, Stanford, California 94305

David W. Chandler
Combustion Research Facility, Sandia National Laboratories, Livermore. California 94551

(Received 6 October 1995; accepted 6 December 1995)

The photolysis of methane is studied using photofragment imaging techniques. Our study reveals that the photolysis of methane proceeds via many different pathways. The photofragment imaging technique is used to resolve and characterize these various pathways and provides therefore unique insight into the dynamical processes that govern this photodissociation. The formation of H-atom photofragments following absorption of a Lyman-α photon, and H_2 photofragments following absorption of two ultraviolet photons (λ=210–230 nm) are studied. The measured H-atom photofragment images reveal that a channel that produces fast H atoms concomitant with methyl fragments is dominant in the Lyman-α photolysis of methane. This channel leads to an anisotropic recoil of the fragments. A secondary channel is observed leading to the formation of somewhat slower H atoms, but an unique identification of this second channel is not possible from the data. At least part of these slower H atoms are formed via a channel that produces H atoms concomitant with CH and H_2 photofragments. The recoil of these slower H atoms appears to be isotropic. The measured, state-resolved $H_2(v,J)$, photofragment images reveal that two channels lead to H_2 photofragments from the two-photon photolysis of methane: a channel that leads to H_2 products concomitant with methylene fragments; and a channel that leads to H_2 products concomitant with CH and H fragments. $H_2(v,J)$ rotational and vibrational distributions are measured for each of these two channels separately. The H_2 products formed via the H_2+CH_2 channel are rotationally and vibrationally highly excited, whereas those formed via the H_2+CH+H channel are rotationally and vibrationally cooler. Rotational distributions of H_2 formed via the H_2+CH+H channel are well reproduced by Boltzmann distributions. Results on D_2 elimination following two-photon photolysis of CD_4 are in general similar and in qualitative agreement with the results on CH_4. © *1996 American Institute of Physics.* [S0021-9606(96)03810-3]

INTRODUCTION

Knowledge about the (photo) dissociation pathways of the methane molecule is of fundamental importance as it is of central importance to organic chemistry, and it is the prototypical molecule having tetrahedral symmetry. Methane photolysis is also of atmospheric interest as methane is quite abundant in the upper atmosphere of the earth and the atmospheres of other planets.[1–3] In the upper atmosphere of the earth and in other planetary atmospheres, photolysis of methane is believed to be one of the primary steps in the synthesis of higher hydrocarbons and other organic molecules. The lowest lying electronic states of methane are located at high energies above the ground state, corresponding in energy to vacuum ultraviolet radiation. Therefore, the photochemistry of methane in the atmosphere is mostly driven by intense solar atomic emission lines, such as Lyman-α radiation. The one-photon absorption spectrum of methane starts at approximately $\lambda<145$ nm. The absorption cross section increases continuously to shorter wavelengths, showing only minor fine structure in the region between λ=100–145 nm.[4–6] This broad absorption region covers transitions to several possible excited states. The lowest excited states of methane are formed from $3s\leftarrow 1t_2$ excitations. The triply degenerate $^1T_2$ states corresponding to the $1t_2 3s$ electronic configuration are expected to be separated into three Jahn–Teller components. Two components have been identified at 9.7 and 10.4 eV.[7,8] The excited states of methane and their vertical excitation energies are not well characterized. It is generally assumed that at photon energies corresponding to Lyman α only the lowest singlet, $^1T_2$, electronic state of methane can be accessed. This $^1T_2$ electronic state is believed to have a short lifetime with respect to dissociation, which partly explains the observed broad and diffuse absorption band. This $^1T_2$ state correlates adiabatically with the $^1CH_2$ $(^1B_1)+H_2$ products.[9,10] Absorption in the region λ=105–115 nm (covered in this study) allows also excitation to higher excited states. As mentioned before, a second $3s\leftarrow 1t_2$ excitation is believed to have a threshold at $\lambda<119$ nm, whereas a $3p\leftarrow 1t_2$ Rydberg excitation manifold is energetically allowed for $\lambda<112$ nm.[7,11]

Some theoretical data are available on excited states and photolysis pathways of methane,[9,10] but experimental data are sparse. Very few experimental studies on methane photolysis have been performed under collision-free conditions.

Downloaded 24 Feb 2012 to 171.64.124.19. Redistribution subject to AIP license or copyright; see http://jcp.aip.org/about/rights_and_permissions

An important variable in atmospheric modeling of the role of methane and its photoproducts is the quantum yields of atomic and molecular hydrogen.[1] Several channels in the photolysis of methane may lead to H and H_2 products. Considering only spin-conserving dissociation channels the following paths may be anticipated:

$$CH_4(^1A_1) \rightarrow CH_3(^2A_2'') + H \quad \Delta E = 4.48 \text{ eV}, \tag{1}$$

$$CH_4(^1A_1) \rightarrow CH_2(a\ ^1A_1) + H_2 \quad \Delta E = 5.01 \text{ eV}, \tag{2}$$

$$CH_4(^1A_1) \rightarrow CH_2(^3B_1) + H + H \quad \Delta E = 9.21 \text{ eV}, \tag{3}$$

$$CH_4(^1A_1) \rightarrow CH_2(a\ ^1A_1) + H + H \quad \Delta E = 9.48 \text{ eV}, \tag{4}$$

$$CH_4(^1A_1) \rightarrow CH(^2\Pi) + H_2 + H \quad \Delta E = 9.07 \text{ eV}. \tag{5}$$

Here, ΔE is the energy required for each particular channel. All energetic data used to obtain the reaction enthalpies are taken from Lias *et al.*[12] and the singlet–triplet splitting in methylene is taken from McKellar *et al.*[13] Earlier results on the photolysis of methane under bulb conditions have been reviewed by Ausloos and Lias.[14] Quantum yields following absorption at Lyman α have been measured by Laufer and McNesby for H_2, $\phi = 0.58$,[15] Rebbert and Ausloos[16] for CH, $\phi = 0.06$, and Slanger and Black[17] for H, $\phi = 1.14$. Additionally, Slanger and Black concluded from their results that the channel producing H atoms concomitant with H_2 and CH, channel (5), is active, and also that the contribution from channel (1), leading to H atoms concomitant with methyl fragments is only minor. Mordaunt *et al.*[18] have studied the formation of H-atom photofragments following absorption of Lyman α using H-atom Rydberg time-of-flight techniques.[19] Mordaunt *et al.*[18] found a value of $\phi = 1.0 \pm 0.5$ for H. The H-atom Rydberg time-of-flight technique also allowed them to measure the kinetic energy release in the photofragments. From these results it was concluded that a very significant part of the H-atom photofragments in the photolysis of methane following absorption at Lyman α is formed concomitant with methyl radicals, in sharp contrast with results of Slanger and Black.[17] Mordaunt *et al.* observed that some of the H-atom photofragments are formed via alternative channels. Although they could not directly assign which of the other possible channels leads to these other H-atom photofragments, they suggested, using RRKM modeling, that decomposition of metastable, internally excited methyl fragments, contributes significantly. Collision-free studies on the formation of molecular hydrogen in the photolysis of methane are even more sparse. Although it is generally assumed that more than one channel is active in the formation of H_2 in the photolysis of methane,[1,14] little evidence exists to prove this assertion.

Measurements of total quantum yields of H and H_2 in the photolysis of methane are not adequate to unravel the dynamics that lead to these products as various different channels (1)–(5) are expected to contribute. In the present work we investigate the channels that lead to formation of atomic and/or molecular hydrogen in the photolysis of methane specifically. The H-atom elimination is studied following photolysis at Lyman α. The H_2 elimination is studied following two-photon absorption ($\lambda = 210$–230 nm). In Fig. 1 an energy diagram is given which shows schematically the reaction energetics for various channels expected in the photolysis of methane for the photon energies used in our study. In our study rotational and vibrational distributions of the H_2 photofragments are measured, using resonance-enhanced multiphoton ionization (REMPI) to detect the $H_2(v,J)$ photofragments. Additionally, angular and speed distributions of the H and $H_2(v,J)$ photofragments are measured, using two-dimensional photofragment imaging techniques.[20] The H and $H_2(v,J)$ photofragment images allow us to determine and characterize the relative contributions of the channels active in the photolysis of methane. We also present results on the D_2 elimination following photolysis of CD_4. These latter results are similar and in qualitative agreement with our results on CH_4.

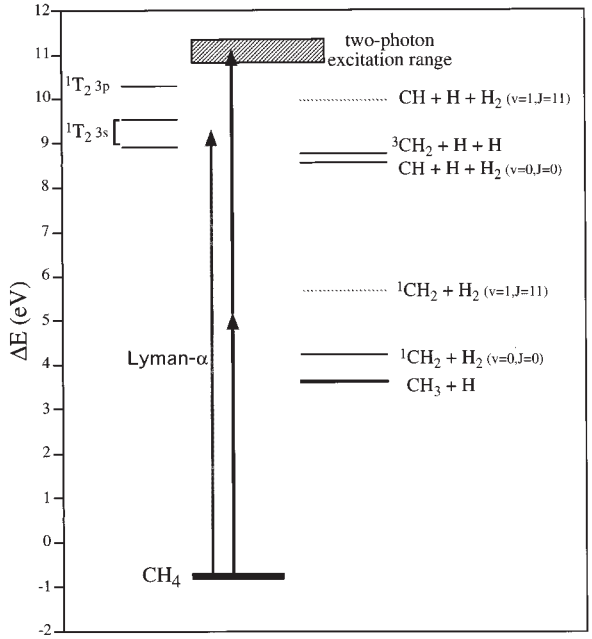

FIG. 1. Schematic energy diagram showing the energetics of possible pathways in the photolysis of methane. The gray arrow indicates the excitation energy deposited in the methane molecule following absorption of a Lyman-α photon; the two black arrows indicate the excitation energy range following absorption of two ultraviolet photons ($\lambda = 210$–230 nm).

EXPERIMENT

The photofragment imaging apparatus used in this study has been described elsewhere in detail.[20,21] Neat methane or perdeuteromethane (backing pressure 6 psig [110 kPa]) is expanded supersonically into a source vacuum chamber through a solenoid valve (General Valve series 9). Approximately 1 cm from the nozzle orifice, the beam is skimmed (Beam Dynamics, orifice 0.8 mm) and collimated by a hole (diameter 1 mm) in the repeller plate.

H-atom elimination of methane is studied following absorption of a Lyman-α photon (121.6 nm). $(1+1')$ Multiphoton ionization of H or D atomic photofragments is accomplished by absorption of a vacuum ultraviolet (vuv) Lyman-α and ultraviolet (uv) photon (364.8 nm). The vuv photon resonantly excites the ground-state H atoms to the $2p$ state. The

Downloaded 24 Feb 2012 to 171.64.124.19. Redistribution subject to AIP license or copyright; see http://jcp.aip.org/about/rights_and_permissions

uv light is generated by frequency mixing the output of an injection-seeded Nd:YAG-pumped dye laser (Spectra Physics GCR5, PDL 2) with the Nd:YAG infrared fundamental light, using KD*P crystals. The bandwidth of the dye laser light is approximately 0.2 cm^{-1}. The vuv Lyman-α light is generated by frequency tripling of the uv light, focused ($f=20$ cm) into a gas cell, in a mixture of krypton and argon adjusted to achieve optimum phase matching.[21,22] The vuv and residual uv laser light pass through a LiF lens ($f=12.7$ cm) into the vacuum chamber where they intersect the molecular beam.

H_2 or D_2 elimination is studied following absorption of two uv photons ($\lambda=210-230$ nm). The laser beam used to dissociate methane by two-photon absorption is also used to multiphoton ionize the $H_2(v,J)$ or $D_2(v,J)$ photofragments state selectively. H_2 and D_2 are detected using (2+1) REMPI spectroscopy via the $E,F\ ^1\Sigma_g^+$ state.[23–26] Ultraviolet light with $\lambda<214$ nm is generated by frequency doubling the injection-seeded Nd:YAG-pumped dye laser light using KD*P crystals. A DCM dye dissolved in methanol is used. Subsequently, the frequency-doubled dye output is sum frequency mixed with the residual dye laser output using appropriate BBO crystals. Ultraviolet light with $\lambda>214$ nm is generated by first frequency doubling the injection-seeded Nd:YAG-pumped dye laser using KD*P crystals. In this case Fluorescein and LDS 590 dissolved in methanol are used. Subsequently, the frequency-doubled dye output is sum frequency mixed with the injection-seeded Nd:YAG fundamental infrared light ($\lambda=1.064$ μm) using appropriate BBO crystals. Throughout the experiments the average uv laser power is kept at approximately 1 mJ per pulse. The uv light is focused ($f=15$ cm) into the molecular beam.

In our experiments the direction of the polarization vector of the laser is chosen to be vertically polarized, i.e., parallel to the face of the position-sensitive ion detector. Following ionization, ions are accelerated along a 20 cm long flight tube and impinge on a two-dimensional, position-sensitive detector. The detector consists of a pair of chevron microchannel plates (Galileo, 7.62 cm diameter) coupled to a fast phosphor screen (P47 Phosphor, 50 ns decay time). The laser, molecular beam, and detection system are all pulsed at 30 Hz. Timing is synchronized by digital delay generators (Stanford Research Systems). To record photofragment ion images the front of the detector is pulsed to detect only one mass peak. The resulting images are recorded using a Peltier-cooled charge-coupled-device (CCD) camera (Photometrics, 576×384 pixels) equipped with a standard 50 mm lens (Pentax). Signal averaging is performed by opening the CCD camera shutter, for approximately 12 000 laser shots, to record a single image. The integrated charge on the CCD is read by the associated camera electronics and transferred for storage and processing to a MIPS RS 3000 computer. Background subtraction is achieved using an image recorded with the laser firing well after the molecular beam gas pulse (typically 1 ms delay). Research grade methane was purchased from Spectra Gasses (Vista, CA), perdeuteromethane (D_4 99%) from Cambridge Isotope laboratories (Andover, MA). Both gases were used without further purification.

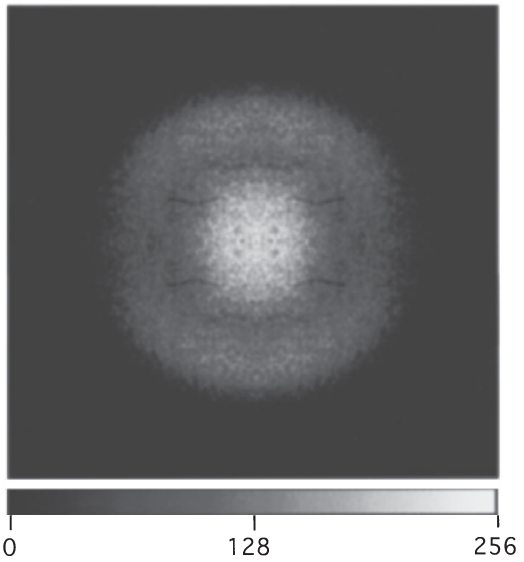

FIG. 2. H-atom photofragment ion image following absorption of a Lyman-α photon in methane. This image was symmetrized (averaged over its four redundant quadrants in order to improve the signal-to-noise ratio of the image). This image is a two-dimensional projection of the recoiling H photofragments.

RESULTS

H atom elimination following absorption at Lyman α

H-atom photofragments are observed when the combined vuv ($\lambda=121.6$ nm) and uv ($\lambda=365$ nm) laser beams intersect with the methane molecular beam. Figure 2 shows the corresponding H-atom photofragment image. To record the image, the laser is scanned over the Doppler profile during data collection. To correct for the background H-atom signal an image recorded with the laser firing well after the molecular beam gas pulse is subtracted. The H-atom photofragment image reveals that (1) two different channels contribute and (2) the recoil of the photofragments is isotropic for the inner channel, but anisotropic for the outer channel. The recorded photofragment images are two-dimensional projections of the three-dimensional recoil of the ionized photofragments. The experimental configuration used dictates that the initial three-dimensional distribution has cylindrical symmetry and therefore the inverse Abel transform[27] can be used to reconstruct, from the two-dimensional image, the intensity distribution through the center of the initial three-dimensional ion cloud.[20] The position of the impinging ions on the position-sensitive detector can be converted to velocity by measuring the displacement of the ions from the center of the image and their arrival time. Velocity distributions are obtained from the inverse Abel transformed image by scaling, appropriately, each pixel of the image.[20]

The three-dimensional speed distribution of H-atom photofragments from methane is shown in Fig. 3(A) and reveals at least two distinct features. Fast H atoms are observed with speeds that peak around 16 km/s and relatively slower H atoms are observed with speeds that peak around 8 km/s. Under the assumption that the H-atom photofragments are formed concomitant with methyl fragments and using mo-

Downloaded 24 Feb 2012 to 171.64.124.19. Redistribution subject to AIP license or copyright; see http://jcp.aip.org/about/rights_and_permissions

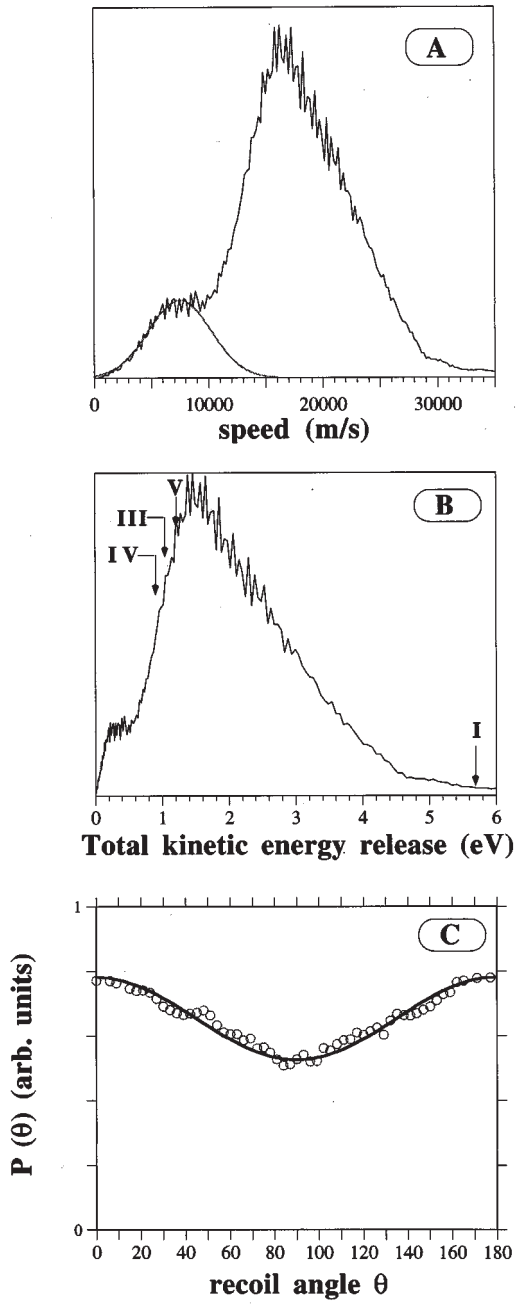

FIG. 3. (A) Speed distribution of H photofragments following absorption of a Lyman-α photon in methane. (B) Kinetic energy release spectrum obtained from the speed distributions of H-atom photofragments. The arrows indicate the energetic thresholds for different channels (1), (3)–(5) in the Lyman-α photolysis of methane. (C) Angular distribution of the H-atom photofragments in the outer ring of the image shown in Fig. 2. This angular distribution was obtained by averaging over the H-atom photofragments with speeds between 12 and 30 km/s.

mentum conservation arguments, the total kinetic energy release into the fragments can be derived from the H-atom speed distributions. The kinetic energy release distribution corresponding to the H-atom elimination from CH_4 is shown in Fig. 3(B). In Fig. 3(B) energetic thresholds are indicated for several channels producing H atoms from the photolysis of methane following absorption of Lyman α. The angular distribution of the H-atom photofragments in the outer ring is shown in Fig. 3(C).

H_2 elimination following two-photon absorption

In methane two-photon absorption, in the range $\lambda = 210$–230 nm, leads to H_2 photofragments. Photofragment images of $H_2(v,J)$ were recorded state selectively for ($v=0$, $J=11$, 13 and 15; $v=1$, $J=0$–19; and $v=2$, $J=0$–11). For CD_4 photofragment images were recorded of $D_2(v,J)$ state selectively for ($v=1$, $J=16$–19; and $v=2$, $J=0$–10). Rotational distributions are obtained by integrating the ion signal intensities over the entire $H_2/D_2(v,J)$ images. In order to obtain rotational distributions corrections to these measured signal intensities must be made which take into account nuclear spin statistics and the differences in the transition moments of the different (2+1) REMPI transitions. Nuclear spin statistics lead to a 3:1 intensity alternations between odd and even J levels of H_2 and to a 1:2 intensity alternation between odd and even J levels of D_2. The relative magnitudes of the transition dipole moments in the (2+1) REMPI scheme are known from calibration experiments,[24] and *ab initio* calculations.[25] In general the calculated results are in good agreement with the experimental data, but cover a wider range of J values and therefore are used here to correct the observed signal intensities. Measured $H_2(v,J)$ signal intensities, and corrected rotational distributions are given in Table I. Measured $D_2(v,J)$ signal intensities, and corrected rotational distributions are given in Table II. In order to measure $H_2(v,J)$ and $D_2(v,J)$ photofragment images the laser was scanned over the Doppler profile. In Fig. 4 photofragment images are shown for $H_2(v=1)$, $J=1$, 11, and 15. The angular distributions of all measured $H_2(v,J)$ products appear to be isotropic. The images shown in Fig. 4 indicate that at least two distinct channels contribute. H_2 speed distributions derived from the inverse Abel transformed images are shown in Figs. 5 and 6, for $v=1$ and 2, respectively. The two features observed in the images are seen in the speed distributions as well. The channel that leads to relatively slow $H_2(v,J)$ products dominates the images at lower J levels, whereas the second channel that leads to relatively faster $H_2(v,J)$ products increases in relative importance with increasing J. For $H_2(v=1), J \geqslant 15$, and for $H_2(v=2), J \geqslant 10$ only the channel leading to the relatively faster H_2 products is observed.

The formation and detection of $H_2(v,J)$ photofragments is the result of a multiphoton absorption process. To form H_2 products methane molecules must absorb two photons. The (2+1) REMPI detection scheme requires absorption of three additional photons by the H_2 products. The dependence of the total $H_2(v,J)$ ion signal on the laser fluence is shown in Fig. 7 for $H_2(v=1, J=9)$. Figure 7 reveals that the H_2 ion intensity is proportional to the laser fluence to the power 3.7 ± 0.4. The (2+1) REMPI detection has been found to be dependent on the laser fluence to the power of 1.5 ± 0.3.[24] Therefore, a laser fluence dependence of approximately two is observed for the H_2 product formation, as expected for a nonresonant two-photon absorption process. Photofragment

Downloaded 24 Feb 2012 to 171.64.124.19. Redistribution subject to AIP license or copyright; see http://jcp.aip.org/about/rights_and_permissions

TABLE I. Rotational distributions H_2 (v,J) photofragments from CH_4.

J	$E_{vib}+E_{rot}$ internal energy (eV)	Measured intensities (arb. units)	Rotational correction	Corrected total intensities (arb. units)	Fraction in fast channel	Fast channel distribution (arb. units)	Slow channel distribution (arb. units)
H_2 $(v=0)$							
11	0.872	2.26	0.911	2.06	0.39	0.793	1.27
13	1.15	2.58	0.867	2.24	0.55	1.23	1.01
15	1.44	2.43	0.812	1.98	0.69	1.37	0.608
17	1.72	1.76	0.812[a]	1.43	0.92	1.31	0.114
$H_2(v=1)$							
0	0.516	0.730	1.09	2.39	0.26	0.611	1.78
1	0.530	5.85	1.08	6.32	0.26	1.63	4.69
2	0.558	2.44	1.08	7.91	0.27	2.17	5.74
3	0.599	8.45	1.07	9.04	0.29	2.67	6.37
4	0.654	3.39	1.05	10.7	0.31	3.37	7.33
5	0.721	10.0	1.04	10.4	0.33	3.44	6.96
6	0.800	3.63	1.02	11.1	0.39	4.30	6.80
7	0.890	9.97	1.01	10.1	0.43	4.32	5.75
8	0.991	3.52	0.987	10.4	0.47	4.88	5.52
9	1.10	9.45	0.967	9.14	0.48	4.41	4.73
10	1.22	3.00	0.945	8.51	0.57	4.84	3.67
11	1.34	9.97	0.921	9.18	0.66	6.08	3.11
12	1.47	2.92	0.959	8.40	0.75	6.27	2.13
13	1.61	7.54	0.870	6.56	0.89	5.83	0.731
14	1.74	1.06	1.09	3.47			
15	1.88	4.95	0.806	3.99	1.0	3.99	0.00
16	2.01	1.15	0.806[a]	2.78	1.0	2.78	0.00
17	2.14	3.17	0.806[a]	2.56	1.0	2.56	0.00
18	2.27	0.770	0.806[a]	1.86	1.0	1.86	0.00
19	2.39	1.28	0.806[a]	1.03	1.0	1.03	0.00
$H_2(v=2)$							
0	1.00	0.950	1.06	3.01	0.53	1.60	1.41
1	1.02	5.53	1.05	5.81	0.56	3.23	2.58
2	1.04	2.37	1.04	7.43	0.56	4.18	3.25
3	1.08	8.81	1.04	9.13	0.58	5.33	3.80
4	1.13	3.12	1.02	9.58	0.62	5.92	3.66
5	1.20	10.1	1.01	10.2	0.68	6.92	3.26
6	1.27	3.16	0.989	9.38	0.71	6.63	2.75
7	1.36	10.4	0.971	10.1	0.78	7.91	2.19
8	1.45	3.20	0.946	9.08	0.85	7.76	1.32
9	1.56	8.18	0.921	7.53	0.92	6.93	0.603
10	1.67	1.98	0.897	5.33	1.0	5.33	0.00
11	1.79	5.13	0.869	4.46	1.0	4.46	0.00

[a]Rotational correction factors are unknown. As an approximate value the rotational correction factor of the nearest J level is used.

images were recorded at different laser fluences for $H_2(v=1, J=9)$. The H_2 speed distributions derived from the images, taken at laser fluences of 500, 700, and 1000 μJ, are shown in Fig. 8. Within the error of the measurements these speed distributions are identical. We conclude that the two observed channels have the same dependence on laser fluence.

DISCUSSION

H atom elimination following absorption at Lyman α

Mordaunt *et al.*[18] have recently studied the H-atom elimination in the Lyman-α photodissociation of methane using the H-atom Rydberg time-of-flight technique. The present study on the H-atom elimination from methane has a similar objective. However, we use photofragment imaging to obtain in a single experiment the speed and angular distributions of the H-atom photofragments. Our H-atom images reveal directly that there are two distinct channels. The speed distributions obtained in our experiments, which are shown in Fig. 3(A), clearly show the two channels in the formation of H-atom photofragments. Following absorption of a $\lambda=121.6$ nm photon several dissociation channels are energetically accessible. The least endothermic channel (1), which produces H atoms concomitant with methyl radicals in the $^2A_2''$ electronic ground state, is endothermic by 4.48 eV. Therefore, following absorption of a Lyman-α photon the maximum possible amount of kinetic energy released into the H and CH_3 fragments is approximately 5.7 eV. The fastest H atoms observed in the H-atom photofragment images have speeds that corresponds to total fragment kinetic energy releases of approximately 5 eV (see Fig. 3). However, the average speed of the H atoms in the outer channel corresponds to a total fragment kinetic energy of approximately

Downloaded 24 Feb 2012 to 171.64.124.19. Redistribution subject to AIP license or copyright; see http://jcp.aip.org/about/rights_and_permissions

TABLE II. Rotational distributions D_2 (v,J) photofragments from CD_4.

J	$E_{vib}+E_{rot}$ internal energy (eV)	Measured intensities (arb. units)	Rotational correction	Corrected total intensities (arb. units)	Fraction in fast channel	Fast channel distribution (arb. units)	Slow channel distribution (arb. units)
D_2 $(v=1)$							
16	1.25	3.240 0	0.880	2.85	0.60	1.72	1.13
17	1.34	1.670 0	0.870	2.90	0.62	1.79	1.11
18	1.44	3.370 0	0.870[a]	2.93	0.72	2.11	0.820
19	1.54	1.440 0	0.870[a]	2.51	0.74	1.86	0.644
$D_2(v=2)$							
0	0.728	0.845 00	1.03	0.870	0.34	0.293	0.577
1	0.734	0.972 00	1.03	2.00	0.34	0.678	1.32
2	0.748	2.636 8	1.02	2.70	0.34	0.918	1.78
3	0.769	1.952 0	1.02	3.98	0.36	1.41	2.57
4	0.796	5.038 0	1.01	5.10	0.38	1.93	3.17
5	0.830	2.754 0	1.01	5.54	0.39	2.16	3.38
6	0.870	5.574 1	0.998	5.56	0.40	2.23	3.33
7	0.917	2.639 0	0.988	5.21	0.43	2.24	2.97
8	0.969	5.272 8	0.977	5.15	0.47	2.41	2.74
9	1.03	2.701 0	0.965	5.21	0.50	2.61	2.61
10	1.09	5.346 0	0.952	5.09	0.55	2.78	2.31

[a]Rotational correction factors are unknown. As an approximate value the rotational correction factor of the nearest J level is used.

1.5 eV. All the H atoms in the outer, fast channel are formed exclusively concomitant with electronic ground state CH_3 ($^2A_2''$) fragments: Based on energy conservation other channels and/or the formation of electronically excited methyl fragments cannot lead to these fast H atoms. The deduced, average amount of internal energy deposited in the CH_3 fragments, as derived from the kinetic energy release spectrum, is high, i.e., approximately 4.2 eV. Thus for the outer channel, the fraction of available energy deposited in translational energy, f_{trans}, is 0.25, whereas the fraction deposited in internal energy, $f_{int}=f_{vib}+f_{rot}$, is 0.75.

Methyl fragments with more than 4.7 eV of internal energy may decompose spontaneously into $CH+H_2$ or when a little more internal energy is available into CH_2+H. Interestingly, the outer channel in the speed distribution drops sharply at the threshold energies for these processes, i.e., for kinetic energy releases below 1 eV. This drop may be an indication that one or more of the channels (3), (4), and (5) start to contribute to the formation of H-atom photofragments at their energetic thresholds [see Fig. 3(B)]. Further decomposition of highly excited methyl fragments may lead to additional H and/or H_2 photofragments via channels (3), (4), and (5). These H atoms can be formed, in principle, in a simultaneous or stepwise breaking of bonds in methane. If the secondary H atoms are formed via a stepwise process the calculated fragment kinetic energy release in Fig. 3(B) must be slightly adjusted, but by no more than 3%. The H-atom photofragment image and speed distribution clearly reveal a second channel that produces relatively slower H atoms. As shown in Fig. 3(B) the onset of this channel corresponds closely with the thresholds of channels (3), (4), and (5). These three channels, which all produce H atoms, have nearly the same energetic thresholds. From our H-atom photofragment images we are not able to resolve which of these channels contributes to the observed signal, but our results for the H_2 elimination, which are discussed below, do indicate that channel (5) is a significant channel in the photolysis of methane. We estimate that the slow channel contributes approximately 13%±5% to the total of the H-atom photofragments in the photolysis of methane at Lyman α. This estimate implies that the rest, 87%±5% of the H atoms are formed concomitant with methyl radicals.

The images show that the faster H-atom photofragments result from an anisotropic recoil, whereas the recoil of the slower H-atom photofragments appears to be isotropic. The angular distribution of photofragments can be described by[28]

$$I(\theta)\approx 1+\beta_2 P_2(\cos\theta), \tag{6}$$

where $P_2(\cos\theta)$ is the second order Legendre polynomial and β_2 is the anisotropy parameter. In Fig. 3(C) the experimentally measured angular distribution of the H-atom photofragments in the outer ring of the image in Fig. 2, is shown together with a fit to this data using Eq. (6). A best fit to the angular distribution of the H-atom photofragments in the outer ring of the image is obtained with an anisotropy parameter, β_2, of 0.28. The observed anisotropy of the fast channel may be caused by the symmetry of the electronic states involved and/or by the relatively short lifetime of the excited methane molecules, i.e., when the methane molecules rotate substantially prior to dissociation anisotropy of the photofragments will be partly washed out.

Our results and those of Mordaunt *et al.*[18] both reveal two distinct channels in the H-atom elimination from methane following absorption at Lyman α. We have measured the speed and angular distributions of the photofragments and find that the recoil of the fast H atoms is anisotropic, the channel leading to slower H atoms is isotropic. By measuring the complete H-atom photofragment three-dimensional distribution we not only obtain the angular and speed distributions of the H-atom photofragments but we also are able to

Downloaded 24 Feb 2012 to 171.64.124.19. Redistribution subject to AIP license or copyright; see http://jcp.aip.org/about/rights_and_permissions

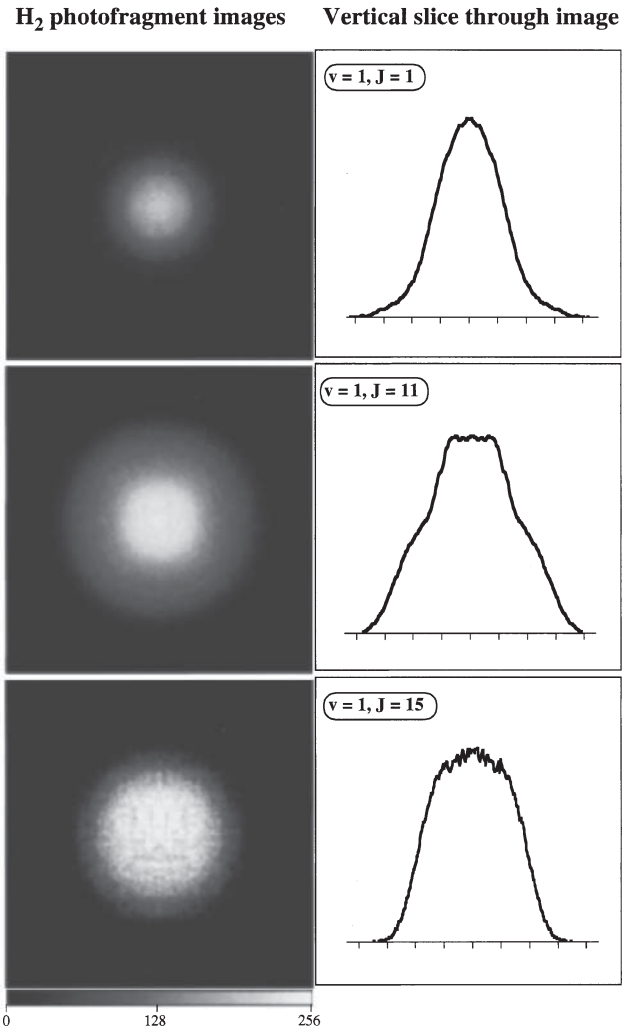

FIG. 4. H_2 photofragment ion images following two-photon (uv) absorption ($\lambda = 210-230$ nm) in methane. These images are two dimensional projections of the recoiling H_2 photofragments. From the top to the bottom are displayed the ion images of $H_2(v=1, J=1)$, $H_2(v=1, J=11)$, and $H_2(v=1, J=15)$. On the right are shown intensity distributions along a vertical slice through the center of the images.

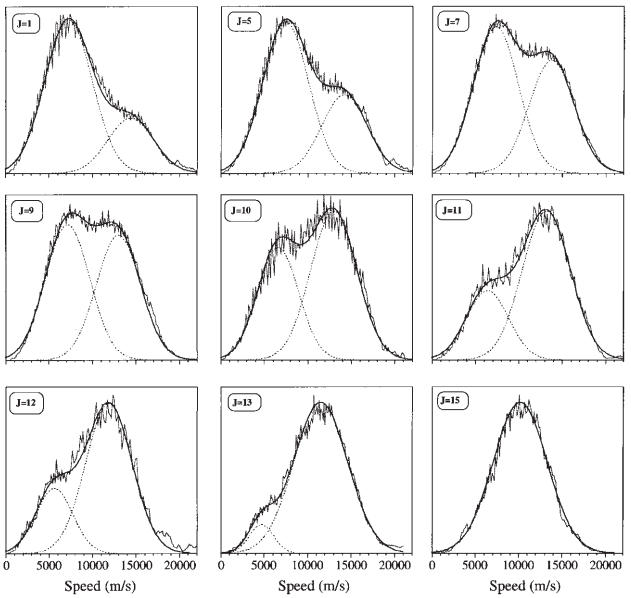

FIG. 5. $H_2(v=1, J)$ speed distributions. Each frame shows the speed distribution of a particular rotational level J. The gray lines are the observed speed distributions, the dashed lines are Gaussian fit functions used to model the speed distributions, and the solid black line is the resulting fit to the speed distribution (see the text for details).

quantify the ratio of H atoms formed concomitant with methyl radicals [channel (1)] and H atoms formed via three-body dissociation channels (3)–(5). We find that channel (1) is the most dominant channel leading to H-atom photofragments. Previous models used to model the chemistry of the upper atmosphere and various planets[1,29] have assumed that channel (1) can be neglected in the photolysis of methane. Our studies reveal that this assumption is not correct.

H_2 elimination following two-photon absorption

Two-photon absorption, which deposits between 10.8 and 11.8 eV of energy in the methane molecule, leads to H_2 photofragments. The recorded $H_2(v,J)$ photofragment images reveal that there are two distinct speed groups of H_2 products. Ignoring the spin-forbidden formation of triplet methylene, the least endothermic dissociation channel of methane that leads to H_2 products is channel (2). As approximately 5.7 eV is available for product excitation following two-photon absorption and formation of singlet CH_2+H_2 this channel will lead to highly internally or translationally excited photofragments. The observed fast channel in the $H_2(v,J)$ photofragment images peaks at speeds of typically 13 km/s. This speed corresponds to a kinetic energy release into the fragments of approximately 2 eV, substantially less than the energetic limit of 5.7 eV. Based on energy conservation the fast channel observed in the images can coincide only with formation of CH_2+H_2. Our data reveal that channel (2) leads to high internal excitation of not only the H_2 products, but also the CH_2 fragments. The slower channel in the H_2 photofragment images corresponds with an average kinetic energy release into the fragments of approximately 0.25 eV. One of the most plausible explanations for this channel is the formation of $CH+H+H_2$. This channel is highly endothermic, but the large amount of photolysis energy still makes it accessible. Assuming that only two major channels contribute to the $H_2(v,J)$ photofragment images the speed distributions are fitted to two Gaussian functions. As variables the widths, heights and positions of the two Gaussians were optimized in the fit. Some typical results obtained from these fits are shown in Figs. 5 and 6 for H_2, $v=1$ and $v=2$, respectively. Using this procedure all $H_2(v,J)$ and $D_2(v,J)$ speed distributions could be fitted satisfactorily. Fitting the speed distributions allows us to determine the contributions of the two different channels to the images. Tables I and II show the derived fractions of products in the fast channel for each measured $H_2(v,J)$ and $D_2(v,J)$ level. By knowing the relative contributions of each of the two channels, the rotational distributions for each individual channel

Downloaded 24 Feb 2012 to 171.64.124.19. Redistribution subject to AIP license or copyright; see http://jcp.aip.org/about/rights_and_permissions

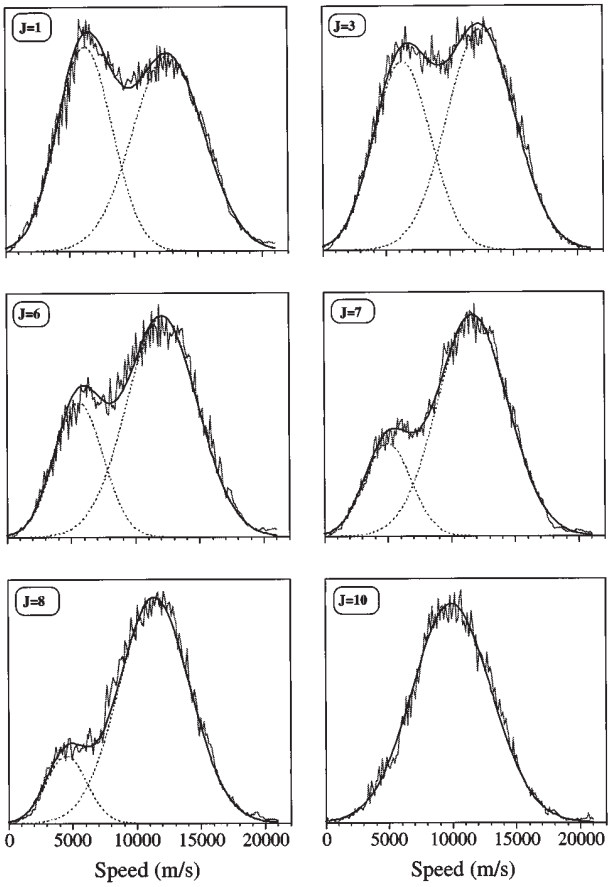

FIG. 6. $H_2(v=2, J)$ speed distributions. Each frame shows the speed distribution of a particular rotational level J. The solid lines are the observed speed distributions, the dashed lines are Gaussian fit functions used to model the speed distributions, and the solid black line is the resulting fit to the speed distribution (see the text for details).

also can be obtained. These rotational distributions are shown in Fig. 9 for $H_2(v=1$ and 2) and in Fig. 10 for $D_2(v=2)$.

The photolysis laser is tuned over an energy range of approximately 1 eV to state-selectively detect the various $H_2(v,J)$ products. The photolysis energy ranges from 10.5 to

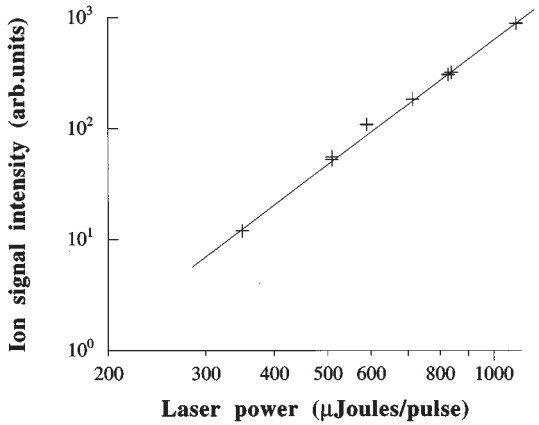

FIG. 7. Log/log plot of the H_2^+ signal intensity versus the laser fluence.

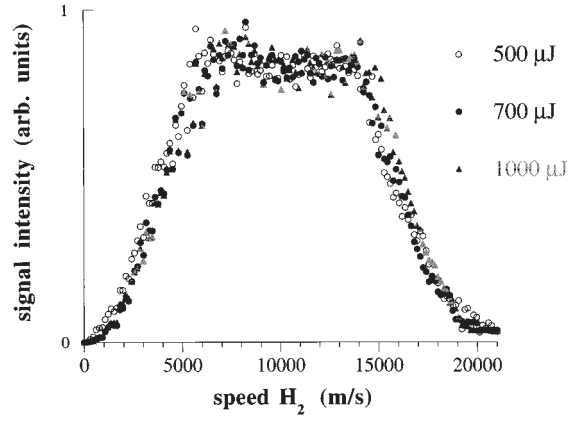

FIG. 8. $H_2(v=1,9)$ speed distributions obtained from ion images measured at three different laser powers of 500 (open circles), 700 (filled circles), and 1000 μJ (gray triangles), respectively.

11.5 eV. As mentioned in the Introduction this amount of excitation energy allows excitation to different excited states of methane.[5,7,8] We do not know exactly which states are excited in the two-photon process but from the smooth rota-

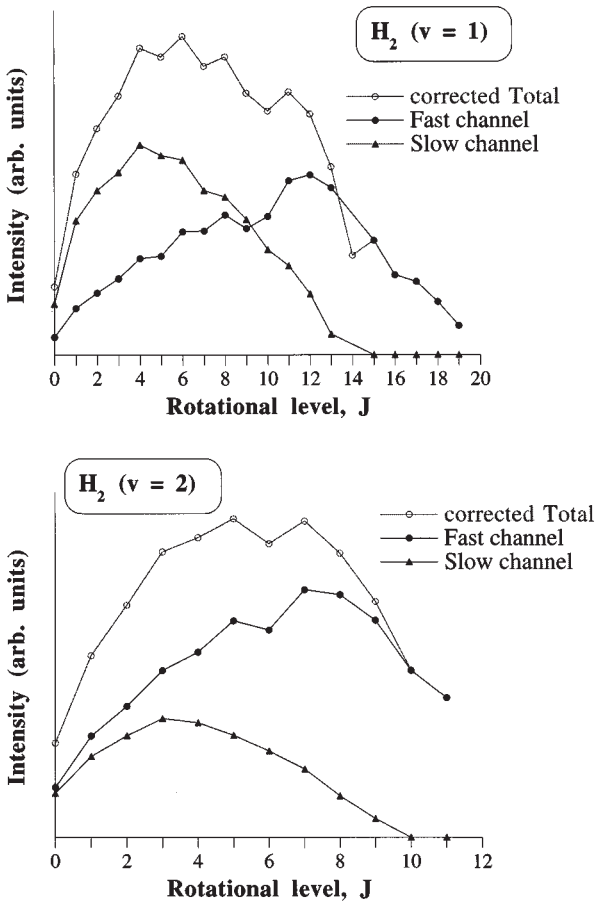

FIG. 9. H_2 rotational distributions in the photolysis of methane for $v=1$ (top) and $v=2$ (bottom). The rotational distributions obtained by integrating the ion signals over the whole of the images are displayed by open circles. The rotational distributions of the fast and slow H_2 channels in the photolysis of methane are shown by filled circles and filled triangles, respectively.

Downloaded 24 Feb 2012 to 171.64.124.19. Redistribution subject to AIP license or copyright; see http://jcp.aip.org/about/rights_and_permissions

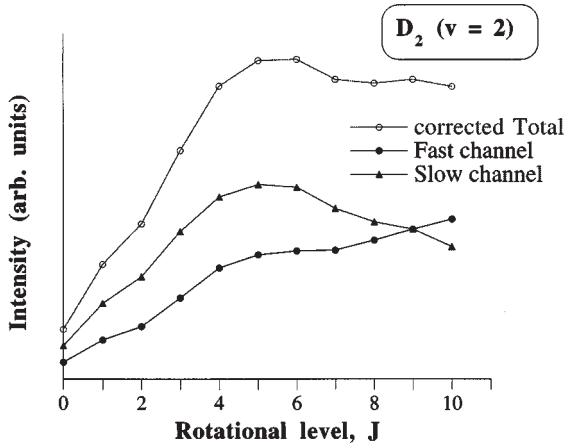

FIG. 10. D_2 rotational distributions in the photolysis of perdeuteromethane for $v=2$. The rotational distributions obtained by integrating ion signals over the whole of the images are displayed by open circles. The rotational distributions of the fast and slow D_2 channels in the photolysis of CD_4 are shown by filled circles and filled triangles, respectively.

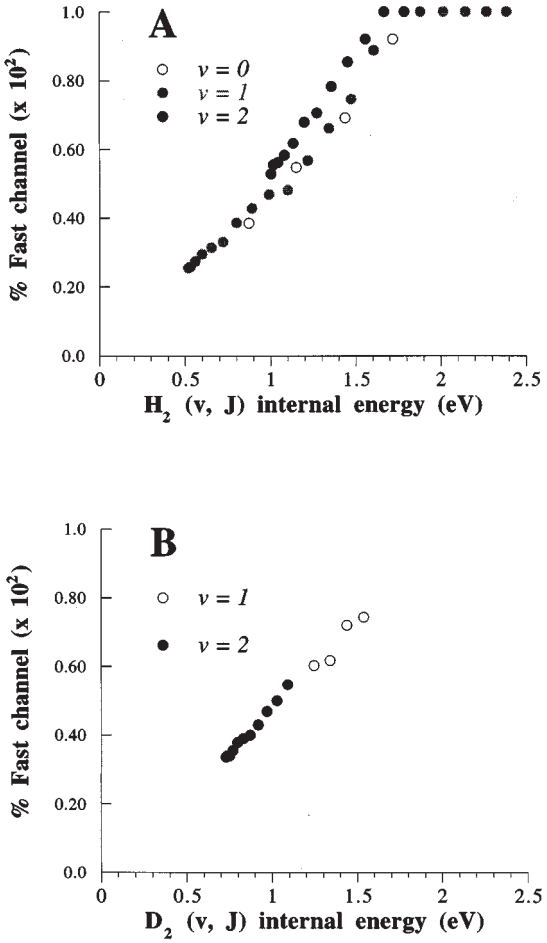

FIG. 11. (A) Percentages of the contribution of the fast channel to the $H_2(v,J)$ photofragment images in the two-photon photolysis of CH_4 plotted versus the internal energy of the corresponding $H_2(v,J)$ products (B) As in (A), but now for $D_2(v,J)$ products in the two-photon photolysis of CD_4.

tional distributions observed we assume that the excitation is fairly broad and unstructured. The one-photon absorption spectrum in this region is fairly continuous, but displays some minor structure around 11 eV, attributed to vibrational levels of the $3p$ Rydberg state.[5] The two-photon absorption spectrum in this energy region is unknown. Galasso[30] has calculated transition probabilities for multiphoton absorption processes in methane. His calculations predict that in the two-photon absorption process $3p \leftarrow 1t_2$ excitations are relatively stronger than $3s \leftarrow 1t_2$ excitations. The observed $H_2(v,J)$ rotational distributions are fairly continuous, for both channels. We interpret the smoothness of the distributions as an indication that the variation in photolysis energy does not effect the observed dynamics significantly. Although the $H_2(v,J)$ products we have detected are formed following absorption at different excitation energies, we believe they are produced via similar dynamic processes, i.e., via the same potential energy surfaces. A possible pathway might be that initial excitation to specific excited states of methane is followed by fast internal conversion to the S_0 ground electronic state.

We derive the relative contributions for each of the two channels from the $H_2(v,J)$ and $D_2(v,J)$ photofragment images and speed distributions. For all studied vibrational levels of H_2 and D_2 the slower channel contributes relatively more in the lower J levels than in the higher J levels. In Fig. 11 the contributions of the fast channel (in %) to the images are plotted versus the internal energy ($E_{vib}+E_{rot}$) of the H_2 [Fig. 11(A)] and D_2 [Fig. 11(B)] products. As seen in Fig. 11 an almost linear correlation exits, up to the cutoff of the slower channel, between the internal energy of the hydrogen molecules and the branching ratio of the two channels. This linear correlation is approximately identical for the different vibrational levels. The fact that the relative contribution of the fast channel increases with increasing internal energy of the products is somewhat counterintuitive. However, the fast channel, which is attributed to the formation of molecular hydrogen concomitant with methylene, is less endothermic, by approximately 4 eV, than the slower channel, which is attributed to the formation of molecular hydrogen concomitant with CH and H. This observed behavior gives additional confidence to the assignments of the fast channel (2) and slow channel (5). The linear correlation between the branching ratio and the H_2 photofragment internal energy might indicate that the two channels are coupled, i.e., the dynamics that lead to channels (2) and (5) occur via the same potential energy surfaces.

ROTATIONAL DISTRIBUTIONS

The fast channel

Dictated by conservation of energy, the outer channel in the images, corresponding to very fast H_2 photofragments, can only be attributed to the formation of molecular hydrogen concomitant with methylene. The rotational distributions observed for this channel, displayed in Figs. 9 and 10, reveal that the H_2 photofragments are formed with high amounts of rotational energy. For instance, the peak in the rotational distribution for this channel for $H_2(v=1)$ is at $J=12$, which

Downloaded 24 Feb 2012 to 171.64.124.19. Redistribution subject to AIP license or copyright; see http://jcp.aip.org/about/rights_and_permissions

corresponds to approximately 1 eV of rotational energy. Approximately 6 eV is available following two-photon absorption and the formation of ground-state CH_2+H_2. As mentioned above the average fragment kinetic energy release for this channel is approximately 2 eV. Conservation of energy implies that the methylene products formed via channel (2) are formed with approximately 3 eV of internal energy. The methylene products may be formed in electronically excited singlet states. The $b\ ^1B_1$ and the $c\ ^1A_1$ states of methylene are approximately 0.9 and 3.4 eV above the $a\ ^1A_1$ state. Emission from the $b\ ^1B_1$ to the $a\ ^1A_1$ state of methylene has been observed following photolysis of methane in the $\lambda=50-132$ nm range.[5,6] The fluorescence quantum yield of this emission reaches its maximum at approximately $\lambda=106$ nm; however, even at this maximum the fluorescence quantum yield is less than 1%.[6] This is taken as evidence that the methylene molecules are predominantly formed in the lowest singlet state, but with large amounts of vibrational and rotational energy. Some theoretical studies have appeared on the reverse reaction, namely, the insertion of singlet methylene into H_2.[31,32] Singlet methylene reacts with molecular hydrogen without a significant activation barrier.[33] When the trajectories calculated to be the minimum energy path for this reaction are run in the reverse order several interesting features are observed. These trajectories predict that the dissociation of methane into singlet methylene and molecular hydrogen follows a stepwise path.[32] Following excitation a hydrogen atom flies from the methane molecule and takes with it a second hydrogen atom, to form a H_2 fragment, as it leaves. Such a path would lead to high rotational excitation of the H_2 products, because of the initial asymmetry of the path. This mechanism is in agreement with the observed high rotational excitation of the molecular hydrogen products.

The slow channel

We attribute the inner channel of the H_2 images to the channel that forms H_2 products concomitant with CH and H products. The H_2 photofragments in this channel are formed with relatively less rotational energy than those in the outer channel, and the fragments' kinetic energy releases do not exceed 0.5 eV. No rotational population is observed in this channel at J levels above 14 and 9, for $H_2(v=1)$ and $H_2(v=2)$, respectively. Formation of $H_2(v=1)$ via channel (5), i.e., concomitant with CH and H fragments, is energetically not allowed for rotational levels with $J>15$, whereas formation of $H_2(v=2)$ is energetically not allowed for $J>10$. The observed cutoff in the rotational distributions are in agreement with the assignment of the inner channel to channel (5). Figure 12 displays the rotational distributions of the slow channel and Boltzmann distributions with rotational temperatures, $T_{\rm rot}$, of 3850, 2150 and 2700 K for $H_2(v=1)$, $H_2(v=2)$, and $D_2(v=2)$, respectively. As can be seen in Fig. 12 these Boltzmann distributions reproduce quite well the observed rotational distributions of the slow channel.

The mechanism for the slow channel can not uniquely be determined from our data as we cannot distinguish between a stepwise or concerted formation of the $H+H_2+CH$ fragments. Mordaunt *et al.*[18] have suggested the possibility that in the photolysis of methane excited methyl radicals are formed that may undergo further unimolecular decomposition into either CH_2+H or $CH+H_2$.[18] Theoretical calculations[34] as well as experimental data[35,36] indicate that the minimum energy paths of both these decomposition reactions involves negligible activation energy. RRKM calculations performed by Mordaunt *et al.* indicate that the decomposition of internally excited ground state methyl

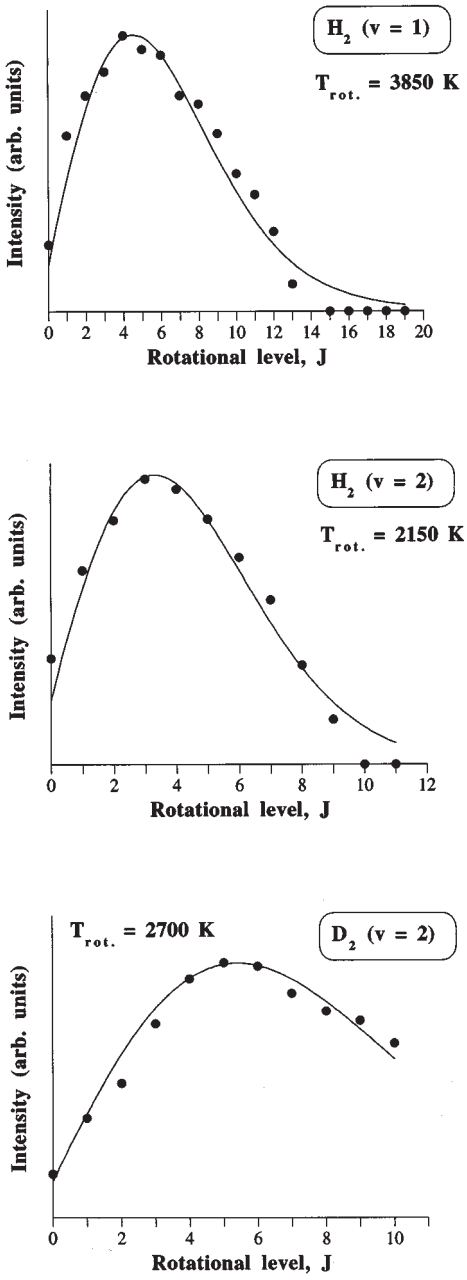

FIG. 12. Rotational distributions in the photolysis of CH_4/CD_4 for the slow H_2/D_2 product channel. From top to bottom are shown $H_2(v=1)$, $H_2(v=2)$, and $D_2(v=2)$ experimental rotational distributions (circles) and Boltzmann distributions with rotational temperatures ($T_{\rm rot}$) of 3850, 2150, and 2700 K, respectively.

Downloaded 24 Feb 2012 to 171.64.124.19. Redistribution subject to AIP license or copyright; see http://jcp.aip.org/about/rights_and_permissions

TABLE III. Vibrational populations (arb. units) H_2 (v) photofragments in the photolysis of CH_4.

v	Fast channel	Slow channel
1	67.0	65.3
2	66.2	24.8

radicals into $CH+H_2$ is favored at least by almost 2 orders of magnitude over the decomposition into CH_2+H over the internal energy range between 4.7 and 5.7 eV. From our data it seems plausible that the H_2 products observed in the slow channel in the images and speed distributions are formed via such a mechanism.

Summarizing, we find that the rotational distributions of the fast and slow channel are markedly different. The fast channel in the formation of H_2 products from the photolysis of methane is attributed to the direct formation of molecular hydrogen and singlet methylene. These H_2 products are formed with a very high amount of rotational energy. The $H_2(v,J)$ rotational distributions are smoothly shaped, and no sharp cutoff or structure is observed. The concomitant methylene products are formed with large amounts of internal excitation as well. Based on previous CH_2 fluorescence studies[5,6] we believe that most of the methylene products are formed in their lowest singlet electronic state, but with high amounts of vibrational and rotational excitation. The experimentally observed rotational distributions in the slow channel are markedly cooler and can be modeled well with rotational temperatures. Rotational population in the slow channel is observed to vanish just below the energetic threshold for the formation of $CH+H+H_2(v,J)$. The slow channel is attributed to the formation of H_2 concomitant with CH and H.

VIBRATIONAL DISTRIBUTIONS

Our set of data is not sufficient to obtain full vibrational distributions of the H_2 photofragments in the photolysis of methane. However, relative vibrational populations can be obtained for $H_2(v=1)$ and $(v=2)$. These vibrational populations are obtained by summing the populations in all measured rotational levels for the slow and fast channel separately. However, the vibrational populations are given in Table III and shown graphically in Fig. 13. In general the sensitivity for detection of H_2 using the (2+1) REMPI detection scheme is different for each vibrational level. Typically, vibrational correction factors, which have been determined experimentally and theoretically,[24,25] must be used to obtain vibrational distributions. The vibrational correction factors are approximately equal for H_2, $v=1$ and 2, and therefore we apply no vibrational correction. For $H_2(v=2)$ we expect some rotational population in J levels higher than we have probed. The vibrational population in the fast channel is therefore somewhat underestimated for $v=2$.

For the fast channel the H_2 vibrational population is approximately equal in $v=1$ and 2. For the slow channel the vibrational population in $v=1$ is much higher than in $v=2$.

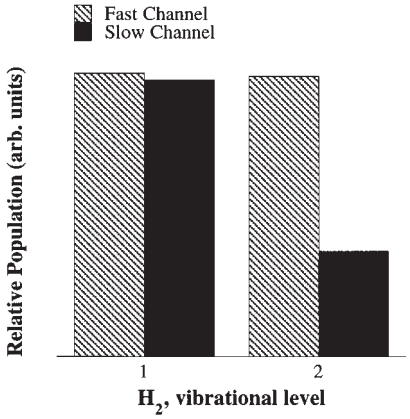

FIG. 13. H_2 vibrational populations in the two-photon photolysis of CH_4. The vibrational populations in the fast and slow H_2 channels in the photolysis of CH_4 are shown by striped and filled bars, respectively.

The fast channel, which leads to H_2 products concomitant with methylene, leads to a significant amount of vibrational excitation in the H_2. From the data shown in Table III and Fig. 13 we infer that there will be population in $v>2$ levels as well. All rotational levels that are energetically accessible for the slow channel in both $v=1$ and 2 are probed. The slow channel leads to much less vibrational excitation of the H_2 products than the fast channel.

The relative importance of channels (2) and (5) in the photolysis of methane can be deduced from our data for $v=1$ and $v=2$. It is observed that both channels (2) and (5) contribute approximately equally to the formation of H_2 products in $v=1$, whereas in $v=2$ channel (2) contributes approximately three times more than channel (5). We have not probed all energetically accessible and/or populated rotational and vibrational levels, and therefore we cannot determine the total yields of the two channels. Our data show, however, that the importance of channel (2), i.e., the formation of methylene concomitant with H_2 is of the same order as that of channel (5), i.e., the formation of H_2 concomitant with CH+H.

CONCLUSIONS

We have studied the photolysis of methane using photofragment imaging to learn about the formation of H-atom photofragments following absorption of a Lyman-α photon, and the formation of H_2 photofragments following two-photon absorption ($\lambda=210$–230 nm). We have determined the speed and angular distributions of the H and H_2 photofragments, as well as rotational and vibrational distributions of the H_2 photofragments. Our study reveals that the vacuum ultraviolet photolysis of methane proceeds via several different pathways. The photofragment imaging technique allows us to unravel and characterize various pathways that lead to H and H_2 photofragments and provides new insight into the dynamical processes that govern this photodissociation.

We find that the most significant channel in the formation of H-atom photofragments in the photolysis of methane

Downloaded 24 Feb 2012 to 171.64.124.19. Redistribution subject to AIP license or copyright; see http://jcp.aip.org/about/rights_and_permissions

is channel (1), i.e., the formation of H atoms concomitant with methyl fragments. The methyl fragments formed via this channel are hot and have an average internal energy of approximately 4 eV. The recoil of the photofragments formed via this channel is anisotropic and can be described by an anisotropy parameter, β, of 0.28. A second channel is observed to lead to slower H-atom photofragments. These H-atom photofragments are formed via the channels (3), (4), and/or (5). The recoil of these slower H-atom photofragments is isotropic. From our H-atom photofragment images alone, we cannot directly unravel to which extent channels (3), (4), and/or (5) contribute.

The $H_2(v,J)$ photofragment images reveal that there are two channels leading to molecular hydrogen in the photolysis of methane. From the images we determine the relative contributions from these channels for each $H_2(v,J)$ product. One channel leads to relatively fast H_2 products, which are formed simultaneous with CH_2 fragments. The rotational distributions of the $H_2(v,J)$ products in this channel (2) are very hot, i.e., $H_2(v,J)$ products with more than 1.8 eV of rotational energy are observed. The methylene products formed via channel (2) are formed with an average of approximately 3 eV of internal energy. The second channel leading to H_2 products is most probably channel (5), i.e., the formation of H_2 products concomitant with CH and H. This assignment is consistent with the observed cutoff in the rotational distributions. The rotational distributions for this channel are markedly cooler and can be described by Boltzmann rotational temperatures of $T_{\mathrm{rot}}=3850$ and 2150 K for $v=1$ and 2, respectively. The observation of this channel in the formation of H_2 products implies that this channel is also responsible for the formation of H-atom photofragments. The ratio of these two channels, which both lead to H_2 products is found to be strongly dependent on the internal energy of the $H_2(v,J)$ products.

In summary, our results on the photolysis of methane reveal that channel (1), i.e., the formation of H atoms concomitant with methyl fragments, is far more important, by a factor of 6, than the summed contributions of all alternative channels that lead to H-atom photofragments [channels (3), (4), (5)). We estimate, from extrapolation of our limited $H_2(v,J)$ data set, that in the formation of H_2 photofragments, channel (2), i.e., the formation of H_2+CH_2, is somewhat more important, by a factor of approximately 2, than channel (5), i.e., the formation of H_2+CH+H. If we combine these results and assume no contributions from channel (3) and (4), the formation of $^{1,3}CH_2+H+H$, we estimate that channel (1) is approximately three times more important than channel (2), and six times more important than channel (5). To the extent that the channels (3) and/or (4) contribute to the observed slow H atoms (13% of the total) the relative contributions of channel (5) and (2) will diminish.

ACKNOWLEDGMENTS

A.J.R.H. thanks the Associated Western Universities, Inc. for an AWU-DOE fellowship. This work was supported by the U.S. Department of Energy, Office of Basic Energy Sciences, Division of Chemical Sciences and in part by the U.S. National Science Foundation under NSF CHE-9322690.

[1] J. S. Levine, *The Photochemistry of Atmospheres* (Academic, New York, 1985).
[2] R. P. Wayne, *Chemistry of Atmospheres* (Oxford University, New York, 1991).
[3] L. M. Lara, R. D. Lorenz, and R. Rodrigo, Planet. Space Sci. **42**, 5 (1994).
[4] H. Okabe, *Photochemistry of Small Molecules* (Wiley, New York, 1978).
[5] L. C. Lee and C. C. Chiang, J. Chem. Phys. **78**, 688 (1983).
[6] G. Ma, M. Suto, and L. C. Lee, J. Quant. Radiat. Transfer. **44**, 379 (1990).
[7] M. B. Robin, *Higher Excited States of Polyatomic Molecules* (Academic, New York, 1974).
[8] M. G. Curtis and I. C. Walker, J. Chem. Soc., Fraday Trans. 2. **85**, 659 (1989).
[9] S. Karplus and R. Bersohn, J. Chem. Phys. **51**, 2040 (1969).
[10] M. S. Gordon and J. W. Caldwell, J. Chem. Phys. **70**, 5503 (1979).
[11] H. U. Lee and R. Janoschek, Chem. Phys. **39**, 271 (1979).
[12] S. G. Lias, J. E. Bartmess, J. F. Liebman, J. L. Holmes, R. D. Levin, and W. G. Mallard, J. Phys. Chem. Ref. Data. **17**, suppl. 1, (1988).
[13] A. R. W. McKellar, P. R. Bunker, T. J. Sears, K. M. Evenson, R. J. Saykally, and S. R. Langhoff, J. Chem. Phys. **79**, 5151 (1983).
[14] P. J. Ausloos and S. G. Lias, Annu. Rev. Phys. Chem. **22**, 85 (1971).
[15] A. H. Laufer and J. R. McNesby, J. Chem. Phys. **49**, 2272 (1968).
[16] R. E. Rebbert and P. Ausloos, J. Photochem. **1**, 171 (1972).
[17] T. G. Slanger and G. Black, J. Chem. Phys. **77**, 2432 (1982).
[18] D. H. Mordaunt, I. R. Lambert, G. P. Morley, M. N. R. Ashfold, R. N. Dixon, L. Schineider, and K. H. Welge, J. Chem. Phys. **98**, 2054 (1993).
[19] M. N. R. Ashfold, I. R. Lambert, D. H. Mordaunt, G. P. Morley, and C. M. Western, J. Phys. Chem. **96**, 2938 (1992).
[20] A. J. R. Heck and D. W. Chandler, Annu. Rev. Phys. Chem. **46**, 335 (1995).
[21] T. N. Kitsopoulos, M. A. Buntine, D. P. Baldwin, R. N. Zare, and D. W. Chandler, Science. **260**, 1605 (1993).
[22] R. Hilbig and R. Wallenstein, IEEE J. Quantum Electron. **QE-19**, 194 (1983).
[23] E. E. Marinero, R. Vasudev, and R. N. Zare, J. Chem. Phys. **78**, 692 (1983).
[24] K.-D. Rinnen, M. A. Buntine, D. A. V. Kliner, R. N. Zare, and W. M. Huo, J. Chem. Phys. **95**, 214 (1991).
[25] W. M. Huo, K.-D. Rinnen, and R. N. Zare, J. Chem. Phys. **95**, 205 (1991).
[26] A. J. R. Heck, W. M. Huo, R. N. Zare, and D. W. Chandler, J. Mol. Spectrosc. **173**, 452 (1995).
[27] R. N. Bracewell, *The Fourier Transform and its Applications* (McGraw-Hill, New York, 1986).
[28] R. N. Zare, Mol. Photochem. **4**, 1 (1972).
[29] B. Bezard, P. N. Romani, B. J. Conrath, and W. C. Macguire, J. Geophys. Res. **96**, 18961 (1991).
[30] V. Galasso, Chem. Phys. **161**, 189 (1992).
[31] C. W. Bauschlicher, Jr., K. Haber, H. F. Schaeffer III, and C. F. Bender, J. Am. Chem. Soc. **99**, 3610 (1977).
[32] M. Sironi, D. L. Cooper, J. Gerratt, and M. Raimondi, J. Am. Chem. Soc. **112**, 5054 (1990).
[33] W. Kirmse, *Carbene Chemistry*, 2nd ed. (Academic, New York, 1971).
[34] M. Aoyagi, R. Shephard, A. F. Wagner, T. H. J. Dunning, and F. B. Brown, J. Phys. Chem. **94**, 3236 (1990).
[35] M. R. Berman and M. C. Lin, J. Chem. Phys. **81**, 5743 (1984).
[36] S. Zabarnick, J. W. Fleming, and M. C. Lin, J. Chem. Phys. **85**, 4373 (1986).

Downloaded 24 Feb 2012 to 171.64.124.19. Redistribution subject to AIP license or copyright; see http://jcp.aip.org/about/rights_and_permissions